

RESEARCH

Open Access



# A comparative proteomic-based study identifies essential factors involved in hair follicle growth in inner Mongolia cashmere goats

Rile Nai<sup>1,2†</sup>, Chongyan Zhang<sup>1,3,4†</sup>, Yuchun Xie<sup>5†</sup>, Duhu Man<sup>2</sup>, Haijun Li<sup>6</sup>, Lina Ma<sup>1,7</sup>, Lu Mi<sup>1</sup>, Meng Zhao<sup>8</sup>, Qier Mu<sup>1</sup>, Lixia Gao<sup>9</sup>, Zhihong Liu<sup>1,3,4\*</sup> and Jinquan Li<sup>1,3,4\*</sup>

## Abstract

Renowned for its invaluable undercoat, the cashmere goat is well known. The growth of cashmere fibre initiates when the relatively inactive telogen stage transitions to the anagen stage, which involves active proliferation. However, the molecular mechanisms responsible for this process are still unclear. Here, SWATH mass spectrometry (MS), a comparative proteomic analysis, was conducted to examine the proteomic alterations in Inner Mongolia cashmere goat skin samples at two different developmental stages (anagen and telogen). In total, 2414 proteins were detected, with 631 proteins showing differential regulation (503 upregulated proteins and 128 downregulated proteins). Bioinformatic analysis revealed that these proteins, which are differentially regulated, play crucial roles in the pathways associated with metabolism and fatty acids according to the GO and KEGG analyses. Furthermore, interactome analysis revealed that differentially regulated keratins have a crucial impact. The localization of KRT25, KRT71, and KRT82 using immunohistochemistry revealed that these proteins were expressed in the secondary hair follicles of cashmere goat skin. The keratin family plays an irreplaceable and important role in the process of hair follicle growth.

**Keywords** Cashmere goat, Proteomics, Hair follicle, Telogen, Anagen

<sup>†</sup>Rile Nai, Chongyan Zhang and Yuchun Xie contributed equally to this work.

\*Correspondence:

Zhihong Liu  
liuzh7799@163.com  
Jinquan Li

lijinquan\_nd@126.com

<sup>1</sup>College of Animal Science, Inner Mongolia Agricultural University, Hohhot 010018, China

<sup>2</sup>College of Agriculture, Hulunbuir University, Hulunbuir 021008, China

<sup>3</sup>Inner Mongolia Key Laboratory of Sheep & Goat Genetics, Breeding and Reproduction, Hohhot 010018, China

<sup>4</sup>Key Laboratory of Sheep & Goat Genetics and Breeding of Ministry of Agriculture, Hohhot 010018, China

<sup>5</sup>College of Animal Science and Technology, Hebei Normal University of Science and Technology, Qinhuangdao 066004, China

<sup>6</sup>College of Veterinary Medicine, Inner Mongolia Agricultural University, Hohhot 010018, China

<sup>7</sup>Inner Mongolia Fengxin Pharmaceutical Co., Ltd., Hohhot 010010, China

<sup>8</sup>Inner Mongolia Academy of Agriculture and Animal Husbandry Sciences, Hohhot 010018, China

<sup>9</sup>Baotou Light Industry Vocational Technical College, Baotou 014035, China



## Introduction

Cashmere is a production of cashmere goat skin with high economic value in the textile industry because it is softer, finer, and lighter than other animal fibres are [1, 2]. Unlike the mechanism of wool production of primary hair follicles (PHFs), cashmere fibres grow from secondary hair follicles (SHFs) and have characteristics of annual cyclic growth, during which they undergo the anagen (a period of cell proliferation), catagen (a period of apoptosis) and telogen (a period of relative mitotic quiescence) phases annually [3, 4]. The cashmere fibre begins to grow after transitioning from the comparatively dormant telogen stage to the actively proliferating anagen stage, and when it enters the catagen phase, the hair follicle (HF) fully stops growing and decreases in diameter and length [5]. Histological studies of SHFs of Inner Mongolia cashmere goats have shown that anagen occurs between April and September, catagen occurs between October and November, and telogen continues until the end of March [6]. The surrounding skin microenvironment, or niche, strictly controls and regulates this sequence of periodic alterations [7]. The transition from the telogen phase to the anagen phase is a complex morphogenetic process of HFs that includes a sequence of reciprocal signals between mesenchymal and epithelial tissues [8, 9]. Exploring the growth process of HFs in more detail is beneficial not only for revealing the mechanism of their formation but also for providing insight into the HF cycle.

The development of HFs is a complex process that necessitates accurate coordination of signals from various cell types in the microenvironment of the skin [7, 10], and some factors have been confirmed to regulate the HF growth process directly or indirectly. For example, these factors may dictate whether an HF will develop on the basis of various combinations of signals, which consist of substances released from the hedgehog, Wnt/wingless, and FGF, BMP, TGF- $\beta$ , and TNF pathways [11–13]. These signals control epidermal-dermal communication [11–13]. Beta-catenin is considered a crucial factor in determining the fate of HFs because of its role in inducing HF formation when epidermal beta-catenin is expressed [14]. Moreover, the apoptosis suppressor BCL-2 may participate in the extension of the growth phase [15], and TGF- $\alpha$  may be involved in the control of the HF shape [8]. However, it is also essential to study these factors overall, as they do not function alone in the skin. There are 12,927 microRNA and 12,865 miRNAs differentially expressed in cashmere goat skin during the SHF transition from telogen to anagen, and they work in the form of a microRNA–miRNA network [16]. Proteins are the ultimate embodiment of life activities [17], and exploration at the proteomic level can provide new insight into the molecular mechanism driving HF regression.

Sequential windowed acquisition of all theoretical fragment ions (SWATH<sup>™</sup>) is a fast data-independent MS/MS acquisition technique that captures all identifiable fragment ions from peptide precursors found in a biological sample in a comprehensive and enduring manner [18–21]. SWATH-MS allows reproducible large-scale protein measurements across diverse cohorts [22]. For a deeper understanding of the intrinsic molecular mechanism of SHF growth, we performed a SWATH-based proteomic analysis to decipher the proteomic signature and its interaction relationships in the skin microenvironment during SHF morphogenesis. The results not only provide a novel protein repository of skin but also help elucidate the relationship between telogen and anagen in SHFs.

## Materials and methods

### Animals

The experimental cashmere goats belonging to the Inner Mongolia cashmere breed and animals used for research were provided by the Aerbasi White Cashmere Goat Breeding Farm located in Inner Mongolia, China [23]. All procedures in this study were performed after the required consent was obtained, and the experiment followed the International Guiding Principles for Biomedical Research involving animals and was approved by the Special Committee on Scientific Research and Academic Ethics of Inner Mongolia Agricultural University, which is responsible for the approval of Biomedical Research Ethics of Inner Mongolia Agricultural University (Approval No: (2020)056, project title: the International Guiding Principles for Biomedical Research involving animals; approval date: May 6th, 2020). For this study, three 2-year-old female Inner Mongolia cashmere goats were randomly selected as replicates in analyses performed in triplicate. The three goats were in good health, with similar developmental, physiological, and feeding conditions. During anagen (September) and telogen (March), samples of dorsal skin were collected approximately 10 to 15 cm from the scapula. Previous studies revealed that the annual development of SHFs in Inner Mongolia cashmere goats raised by the Aerbasi White Cashmere Goat Breeding Farm was the same [24]. Prior to sampling, the site underwent shearing, shaving, and local anaesthesia with 2% lidocaine. Skin samples (1 cm<sup>2</sup>) were collected using a single-use skin biopsy punch. The samples were preserved at -80 °C in the laboratory, and the transportation process of the samples was complete in liquid nitrogen. After the study was finished, the animals were released because the procedures were minimally invasive and euthanasia was not needed.

### Total protein extraction

The same quantity of each skin sample was crushed in liquid nitrogen, and then, 500  $\mu$ l of 1% sodium dodecyl

sulphate (SDS) was added to the lysate. After that, the mixture was incubated at ambient temperature for 20 min before being ultrasonically sonicated for 2 min and then centrifuged at 4 °C and 12,000 rpm for 15 min. A BCA protein assay kit (Biotek, Beijing, China) was used to determine the total protein content in the supernatant. The results of total protein extraction are shown in S1.

#### **Tryptic digestion of total protein**

One hundred micrograms of denatured total protein was treated with a mixture of 200 µl of 10 mM DL-dithiothreitol (DTT) and 8 M urea at 37 °C for 1 h, followed by centrifugation for 40 min at 12,000 rpm. The samples were then treated with 200 µl of 50 mM iodoacetamide (IAA) and incubated at room temperature with the light ray blocked for 30 min before centrifugation for 30 min at 12,000 rpm. To cleave proteins into peptides, the proteins were digested using trypsin (Promega, USA). Following digestion, 100 mM ammonium bicarbonate was added for elution, and the samples were centrifuged at 15,000 rpm for 30 min with a 10 kDa size-exclusion membrane (Sartorius, Germany). The eluates were dried in vacuo.

#### **SWATH-based LC–MS/MS analysis**

An Eksigent NanoLC Ultra 2D Plus HPLC system was linked to a 5600 TripleTOF mass spectrometer for LC–MS/MS analysis (Sciex, Framingham, MA, USA). For the data acquisition of peptide separation by LC–MS–MS (LC–MS–MS–MS), two distinct approaches, information-dependent acquisition (IDA) and SWATH acquisition, were employed.

Peptides weighing approximately 2 µg were injected and separated on a C18 HPLC column (inner diameter: 75 µm × 15 cm). The peptides were separated using a linear gradient of 0.1% formic acid in water (A) and 0.1% formic acid in acetonitrile (B) for 120 min at 500 nL/minute. An MS TOF was collected from 350 to 1800 m/z for IDA, followed by an IDA of MS/MS with automated collision energy selection scanned from 40 to 1800 m/z for 0.05 s per spectrum. The resolution power was 30,000. SWATH–MS interrogated the MS1 mass range of 150–1200 m/z, and MS2 spectra were collected from 100 to 1500 m/z. The MS1 and MS2 scans had nominal resolving powers of 30,000 and 15,000, respectively. Analyst software (Sciex, Framingham, MA, USA) was used to automatically determine the collision energy by considering the m/z window range.

#### **Data analysis**

To acquire a classified spectral collection, we conducted peptide recognition through the Protein Pilot 4.5 application (Sciex, Framingham, MA, USA) utilizing the

UniProt/SWISS-PROT *Capra hircus* database (obtained from <https://www.UniProt.org>; 9925 proteins) with the following configurations: sample type, identification; cysteine alkylation, iodoacetamide; digestion, trypsin; instrument, Triple TOF 5600; ID focus, biological modification; search effort, thorough ID. Peptide detections by ProteinPilot were filtered at a 1% false discovery rate (FDR). In this study, skin peptides regulated at the HF developmental stages of telogen (March) and anagen (September) were detected by Protein Pilot, and we identified the total peptides in both periods (telogen and anagen) by Protein Pilot. The information from Protein Pilot (telogen and anagen) was imported into PeakView software (Sciex, Framingham, MA, USA) to analyse the SWATH database with the ion library created in Protein Pilot [25]. PeakView software processed both targeted and nontargeted data to generate extracted ion chromatograms (XIC). After that, the data were conveyed to Markerview software (Sciex, Framingham, MA, USA) for interpretation and quantitative analysis. Markerview enables quick analysis of the data to identify protein expression changes (up- and downregulation) that have occurred [19]. Principal component analysis (PCA) via Markerview was used to process the data, and the screening criteria for differentially expressed proteins in this study were a *P* value < 0.05 and a fold change > 2 or < 0.5.

#### **GO and KEGG pathway analysis**

To visually examine the role of proteins with altered expression, we used the DAVID gene functional classification tool (<https://david.ncifcrf.gov>) and the CluGo plug-in of Cytoscape software to perform Gene Ontology (GO) analysis and Kyoto Encyclopedia of Genes and Genomes (KEGG) pathway analyses. All of the bioinformatic analyses were deemed significant at a corrected *P* value of 0.05. A bar graph is used to represent the results of the GO enrichment analysis performed on differentially regulated proteins. This graph can be used to visualize the various components of the biological process (BP), cellular component (CC), and molecular function (MF) categories.

#### **Construction of the PPI network**

STRING (<https://string-db.org/>), a web-based bioinformatic platform dedicated to protein–protein interactions (PPIs), provides extensive data on the interactions of proteins. Differentially regulated proteins were uploaded to STRING 11.5 to obtain information on PPIs. The medium confidence interaction score (0.4) was established as the minimal requirement. To generate a visual PPI network, the interactions were imported into the Cytoscape 3.9.0 application. The value of proteins was evaluated by calculating their betweenness centrality.

### Western blotting

A total of 30 µg of protein was separated from each group via 12% SDS-polyacrylamide gel electrophoresis (SDS-PAGE) ( $n=3$  samples/group). After the proteins were transferred to a PVDF membrane (PALL, New York, USA) using a semidry membrane transfer method, they were blocked for 2 h at room temperature with 5% skim milk. The membrane was then incubated overnight at 4 °C with rabbit polyclonal anti-keratin 25 (Abcam, 1:500), rabbit polyclonal anti-keratin 71 (Abcam, 1:500), and mouse monoclonal anti-tubulin (Abcam, 1:1000) antibodies. The membrane was then washed with PBST and incubated for 1 h at 37 °C with a fluorescent-labelled goat anti-mouse secondary antibody and a goat anti-rabbit secondary antibody (LI-COR Biosciences, Inc., Lincoln, NE, USA; 1: 3,000). The immunoreactive bands were examined with a LI-COR® Odyssey near-infrared imager (LI-COR Biosciences, Inc.) after the membranes were washed. ImageJ software was used to quantify the immunoblots, and statistical analyses were conducted using SPSS 23.0 (Chicago, USA). Parametric one-way ANOVA was applied for data examination. The experimental data are expressed as the means  $\pm$  SDs. Statistical significance was considered at  $P < 0.05$ .

### Immunohistochemistry

Fresh skin samples from Inner Mongolia cashmere goats were obtained during the telogen and anagen phases. The samples were first fixed for 24 h in 4% paraformaldehyde. Before being embedded in paraffin, the sections were dehydrated in pure alcohol, and the alcohol was then replaced with benzene. The tissue sample slices, which were 8 µm thick, were subjected to a series of incubations, including xylene for dewaxing, gradient alcohol hydration, and 3% hydrogen peroxide ( $H_2O_2$ ) at room temperature to inactivate endogenous catalase. The samples were then flushed with phosphate-buffered saline (PBS), and antigen retrieval was carried out in citrate buffer, after which the samples were blocked at room temperature for 1 h with 5% bovine serum albumin (BSA). The samples were subsequently incubated with rabbit polyclonal anti-KRT25 antibody (Abcam, 1:50), rabbit polyclonal anti-KRT71 antibody (Abcam, 1:1000), and rabbit polyclonal anti-KRT82 antibody (Affinity, 1:500) overnight at 4 °C. 5% BSA was used as a negative control. The samples were subsequently washed with PBS and incubated with HRP-labelled goat anti-mouse secondary antibody (Beyotime, 1:500) for 1 h at 37 °C. Haematoxylin was used for final staining of the sections, and the results were observed using light microscopy.

## Results

### Proteomic changes in inner Mongolia cashmere goat SHFs during anagen and Telogen

From January to March, the coat of the Inner Mongolia cashmere goat undergoes a period of relative mitotic quiescence (telogen), followed by the initiation of growth in April. The peak period of cashmere growth occurs in August and September [24].

To examine potential proteins associated with the growth phase of cashmere goat skin SHFs, we performed IDA/SWATH-MS proteomic analysis of cashmere goat skin in the stages of anagen (September) and telogen (March). A total of 2414 proteins were detected and measured (S1), and principal component analysis (PCA) of those proteins revealed that proteins in anagen and telogen were distributed at different intervals, indicating that there was a major difference in the proteome between these two stages (Fig. 1a). We compared the proteomic signatures from anagen and telogen, and if the fold changes in these two groups of proteins were greater than 2 or less than 0.5, we considered them to be differentially regulated. Volcano plots of the differentially expressed proteins are displayed using the values of  $\log_2$  (fold change) and  $-\log_{10}$  ( $P$  value) (Fig. 1b). This comparison revealed 503 proteins whose expression differed at least twofold between telogen and anagen, representing the proteins that were upregulated in anagen. There were 128 proteins with a fold change of less than 0.5, representing the downregulated proteins in the anagen phase. The differentially expressed proteins (DRPs) included mainly ribosomal proteins (r-proteins), eukaryotic translation initiation factors (EIFs), keratin (KRT) family members, and S100 family proteins. Comprehensive information on the DRPs is presented in Supplementary Data S2 and S3.

### Functional enrichment analyses of differentially regulated proteins

To assess the biological importance of these DRPs, we performed GO term and KEGG pathway enrichment analyses.

We analysed the GO clustering of the DRPs in BP, CC, and MF terms between anagen and telogen. The results revealed that among the main enriched GO BP terms, cell adhesion was the most significantly enriched process, and most of the DRPs were enriched in the processes of protein transport and folding, RNA processing, and splicing. In addition, the DRPs were enriched in processes directly related to HF growth, such as hair follicle morphogenesis, cell ageing, keratinocyte differentiation, and keratinization (Fig. 2a). In CCs, these DRPs were enriched primarily in the extracellular exosome, cytoplasm, and nucleus (Fig. 2b). With respect to MFs, DRPs were enriched mainly in poly(A) RNA binding, protein binding, and RNA binding (Fig. 2c).

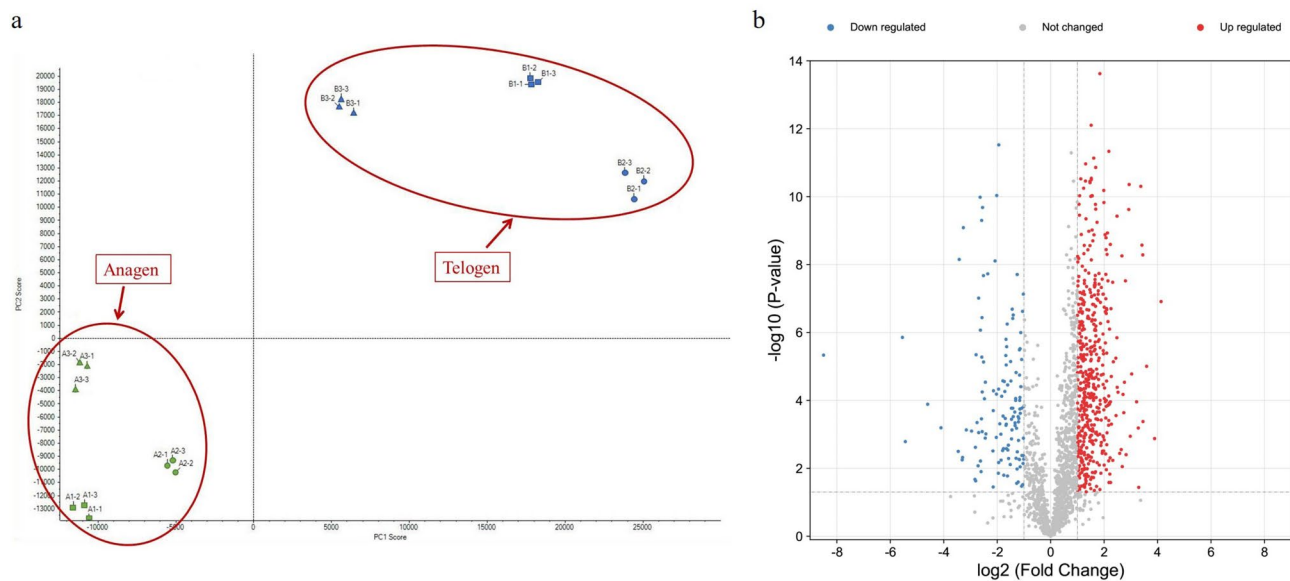


**Fig. 1** Screening of differentially expressed proteins. **(a)** PCA of the remaining period and growth period; 1, 2, and 3 in the figure represent three goats, and -1, -2, and -3 represent technical replicates; **(b)** Volcano plots comparing telogen and anagen. x-axis:  $\log_2$  (fold change), y-axis:  $-\log_{10}$  ( $P$  value). The tag in green represents upregulated proteins in anagen, and the tag in red represents downregulated proteins in anagen

In terms of KEGG pathway information, which is important for understanding the functions of DRPs, metabolism-related pathways, such as the TCA cycle signalling pathway, propanoate metabolism signalling pathway, and protein export, were the top associated pathways (Fig. 2d). In addition, fatty acid-related pathways, such as fatty acid degradation, biosynthesis of unsaturated fatty acids, and fatty acid elongation, were enriched. Furthermore, DRPs were enriched in several pathways related to hair follicle growth, such as the TGF- $\beta$  signalling pathway, the VEGF signalling pathway, and the Wnt signalling pathway [26, 27].

#### Protein–protein interaction (PPI) analysis

For analysis of the interplay among the DRPs, all those proteins were uploaded to STRING 11.5 software to identify the interrelations. Next, the construction of the PPI network was carried out utilizing the Cytoscape software. As illustrated in Fig. 3a, the interaction network consisted of 433 nodes and 2741 edges. In this network, according to the filter criteria, five modules were identified with the MCODE plugin (Fig. 3b–e). Cluster 1 has the highest cluster score of 18.222, consisting of 19 nodes and 164 edges. Cluster 2 is in second place, with a cluster score of 12.833, 13 nodes, and 77 edges. Cluster 3 has a score of 11.500, 13 nodes, and 69 edges, and Cluster 4 has a score of 8.833, 13 nodes, and 53 edges. MCODE analysis of the PPI prediction results of our study revealed that the cluster with the highest score was mainly composed of r-proteins and EIFs (Fig. 3b). The cluster with the second highest score was mainly composed of KRT family members, including KRT35, KRT73, KRT4, KRT82, KIF1,

KRT71, KRT32, KRT85, KRT25, KRT39, KRT28, KRT74, and KRT27 (Fig. 3c).

#### Validation by Western blotting

The keratin cluster (Cluster 2) was the cluster with the highest score. In addition, KRT25 and KRT71 are involved in the BP of hair follicle morphogenesis. Therefore, these two KRTs were selected for Western blotting (WB) verification. Additionally, the index utilized to calculate the relative content of the target proteins was the grey-level ratio between the target proteins and internal controls. The expression of KRT25 and KRT71 in the skin during anagen and telogen is shown in Fig. 4a, and the difference in expression was very notable. The relative contents of the target proteins are shown in Fig. 4b and c. The findings demonstrated that KRT25 and KRT71 expression in anagen was greater than that in telogen, and the trends were similar to those found in SWATH.

#### Localization of KRT25, KRT71 and KRT82 by immunohistochemistry

The expression sites of KRT25, KRT71, and KRT82 in the skin of cashmere goats were determined by immunohistochemistry. After these sites were observed under a light microscope, brown cells were considered positive. The negative results revealed no yellow or brown staining (Figs. 5a and c, 6a and c and 7a and c), and all the immunohistochemistry results revealed that the background staining was light blue or colourless. In contrast, the experimental group exhibited distinct yellow or brown staining, indicating that the immunohistochemistry approach produced a particular immune response

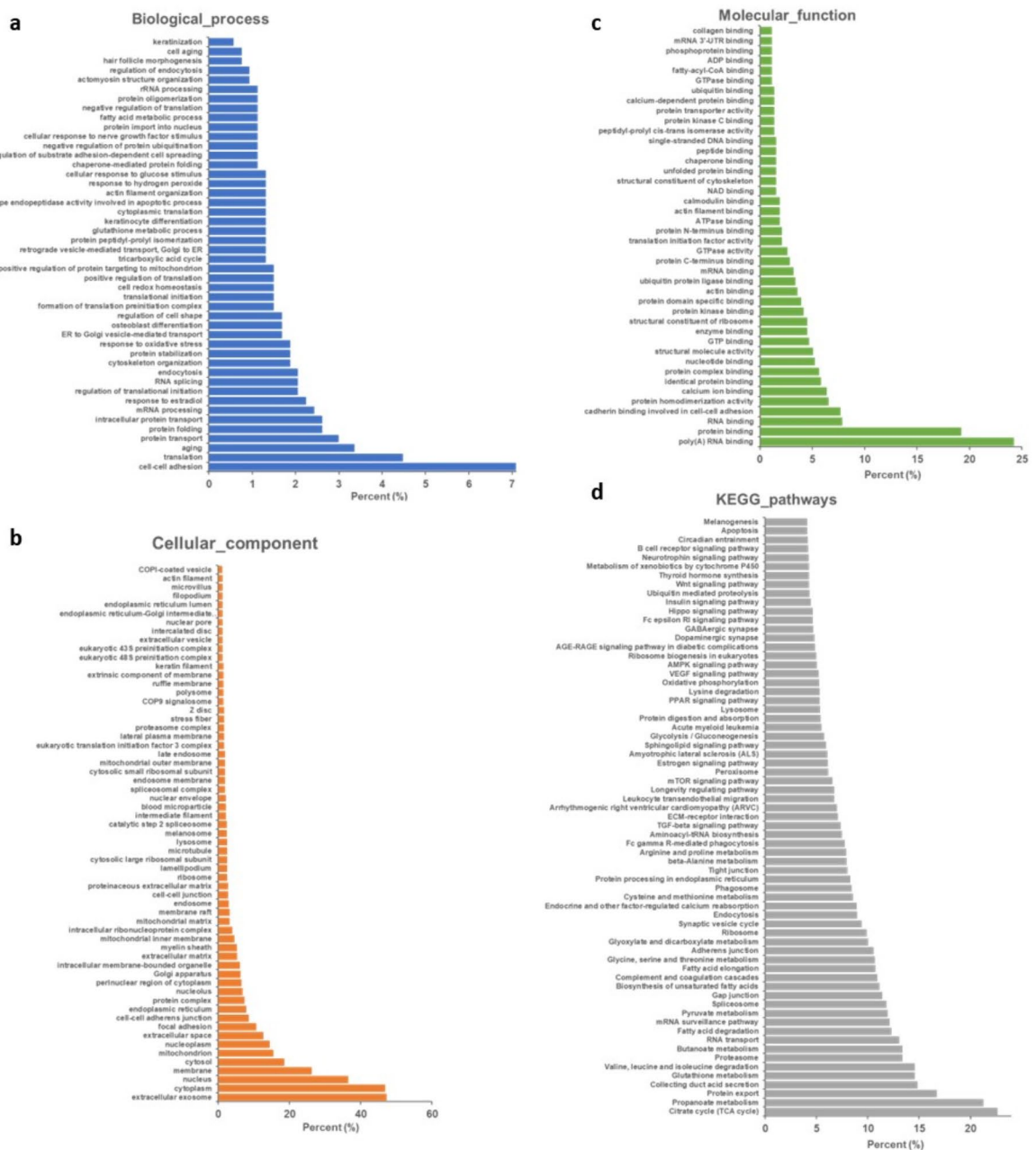


**Fig. 2** Bioinformatic analysis of differentially expressed proteins. **(a)** GO enrichment analysis (BP) of differentially regulated proteins; **(b)** GO enrichment analysis (CC) of differentially regulated proteins; **(c)** GO enrichment analysis (MF) of differentially regulated proteins; **(d)** KEGG pathway analysis of differentially regulated proteins

to KRT25, KRT71, and KRT82 (Figs. 5a and c, 6a and c and 7a and c). As shown in Figs. 5a and c, 6a and c and 7a and c, positive immunohistochemical staining for KRT25, KRT71, and KRT82 was observed in the SHFs of Inner Mongolia cashmere goat skin, with KRT25 in the IRS (Fig. 5a and c), KRT82 in the ORS (Fig. 6a and c), and KRT71 visible in both the IRS and ORS (Fig. 7a and c). The above three members of the KRT family can be found in both telogen and anagen, and the difference in

their expression levels may be because the SHFs in telogen are much shorter than those in anagen.

**Discussion**

The skin, which serves as the external barrier for animals, envelops the whole organism and is dispersed in anatomically distinct niches that provide it with a specialized microenvironment [28]. HFs are important components of the skin, and the development and growth mechanisms of HFs have focused on mammals with single

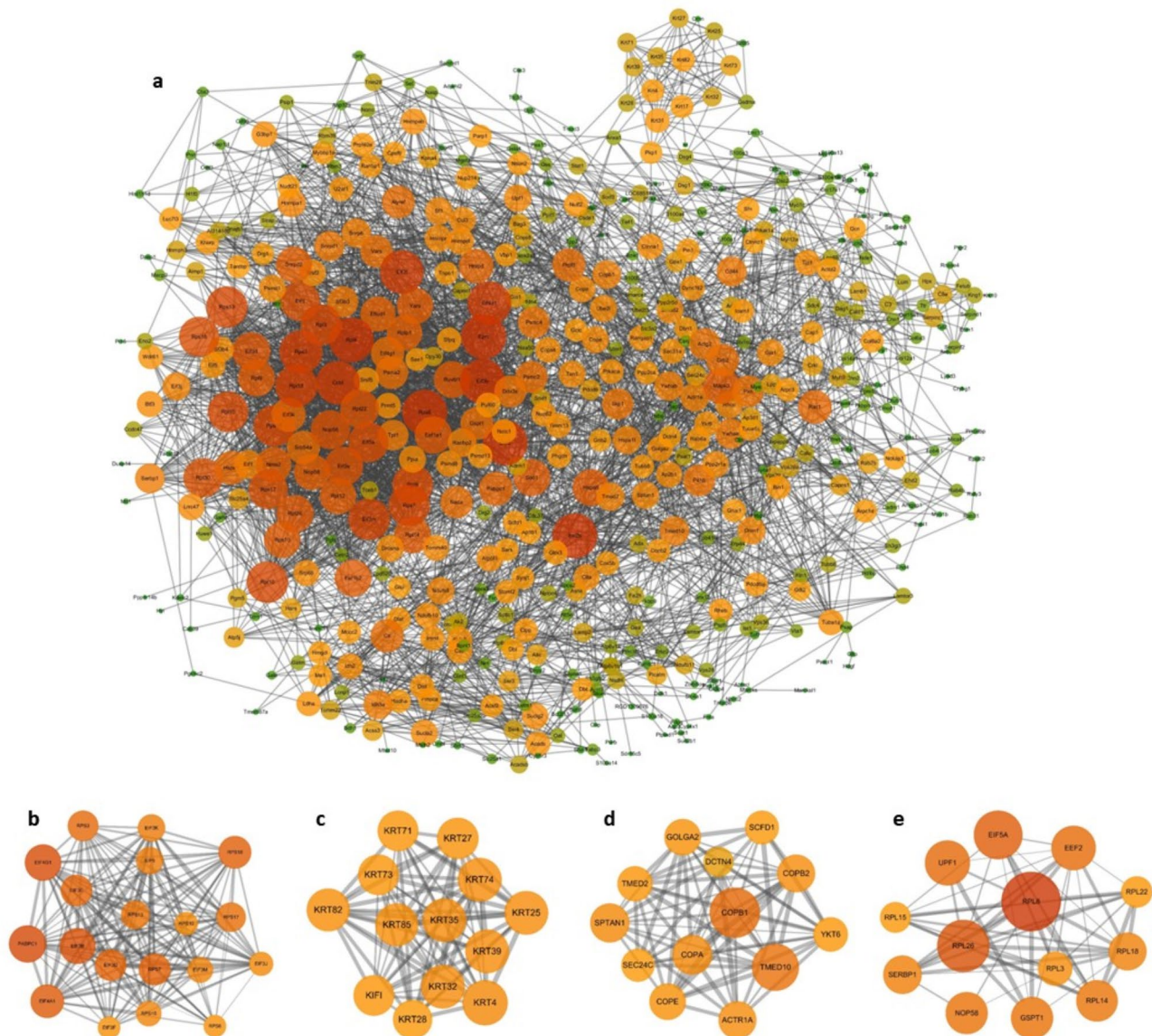


**Fig. 3** Protein–protein interaction network analysis of differentially regulated proteins and **(a)** The interaction network between differentially regulated proteins comprised 433 nodes and 2741 edges. The colour gradient varies depending on the direction of the links characterizing each node, computed as the in/out degree ratio, from red (higher) to green (lower). The spatial network arrangement was obtained by using the Cytoscape prefuse force-directed layout; **(b)** had the highest cluster score (score: 18.222, 19 nodes and 164 edges), followed by Cluster 2; **(c)** (score: 12.833, 13 nodes and 77 edges), Cluster 3; **(d)** (score: 11.500, 13 nodes and 69 edges), and Cluster 4; **(e)** (score: 8.833, 13 nodes and 53 edges)

coats, such as mice and humans [29–33]. The primary, wool-producing follicles of cashmere goats are typically larger, whereas the secondary follicles are smaller and produce softer and finer cashmere. Cashmere goat skin contains more than 90% SHFs, and in addition to PHFs, SHFs follow their internal clock with a noticeable photoperiod-based cycle [34]. Clearly, then, there must be some signals involved in cycling in SHFs, which has no effect on PHFs. A comparative analysis based on differential proteomics of these two periods of anagen and telogen in this study could provide a better understanding of the cyclical growth mechanism of cashmere goats and

offer novel strategies for increasing fine cashmere quality through breeding. The results revealed that 631 proteins were extremely significantly differentially expressed: 503 proteins whose expression was upregulated and 128 proteins whose expression was downregulated.

Since birth, the lifelong cycle growth mode of mammalian HF is initiated. For cashmere goats, SHFs show annual periodicity. Apoptosis of keratinocytes in the matrix, inner root sheath (IRS), and outer root sheath (ORS) leads to rapid degeneration of the lower two-thirds of HF during catagen, whereas bulge HF stem cells evade apoptosis. At the end of catagen, the lower HF undergoes

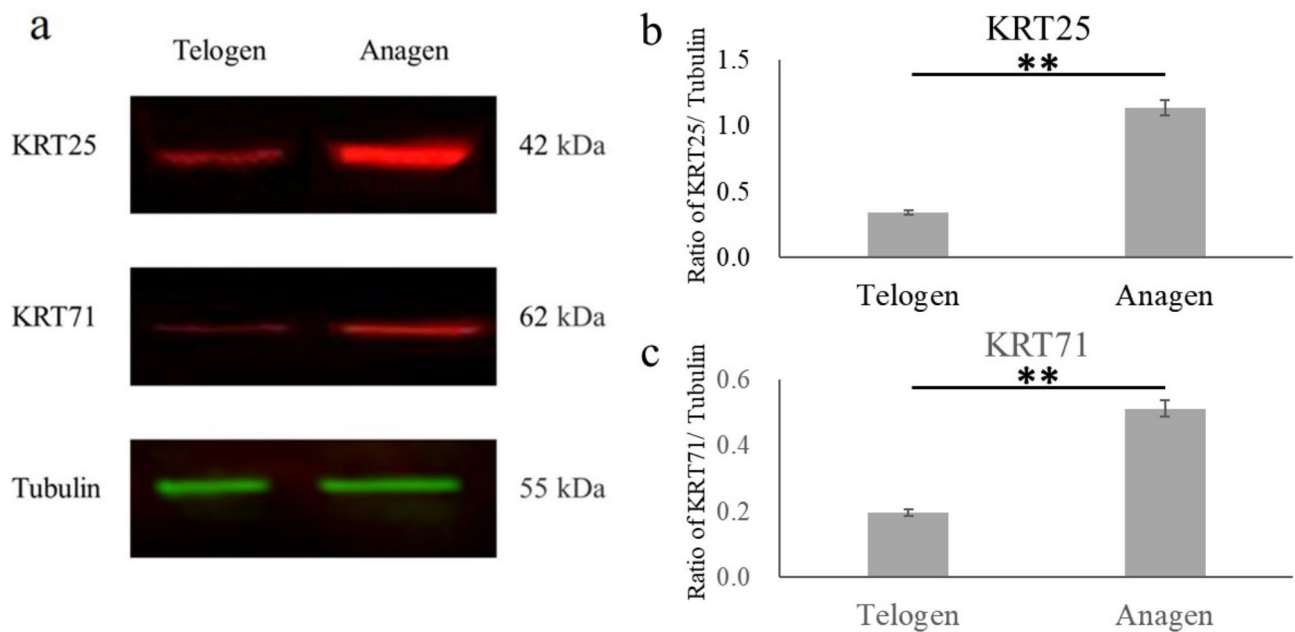


**Fig. 4** Western blotting analysis of the differentially expressed proteins between telogen and anagen phases. **(a)**: Western blotting of KRT25 and KRT71 in skin samples collected during telogen and anagen; **(b and c)**: Relative expression of KRT25 and KRT71 in skin samples collected during telogen and anagen. **\*\*** $P < 0.01$

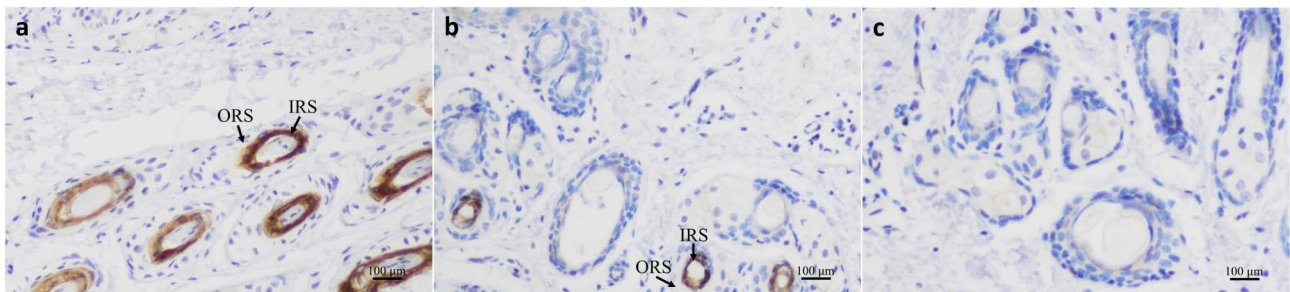


**Fig. 5** Localization of KRT25 in the skin of Inner Mongolian cashmere goats by immunohistochemistry. Brown cells were considered positive. **(a)**: Staining of KRT25 during anagen. (200 x); **(b)**: Staining for KRT25 during telogen. (200 x); **(c)**: Negative control. (200 x). Note: IRS, inner root sheath; ORT, outer root sheath

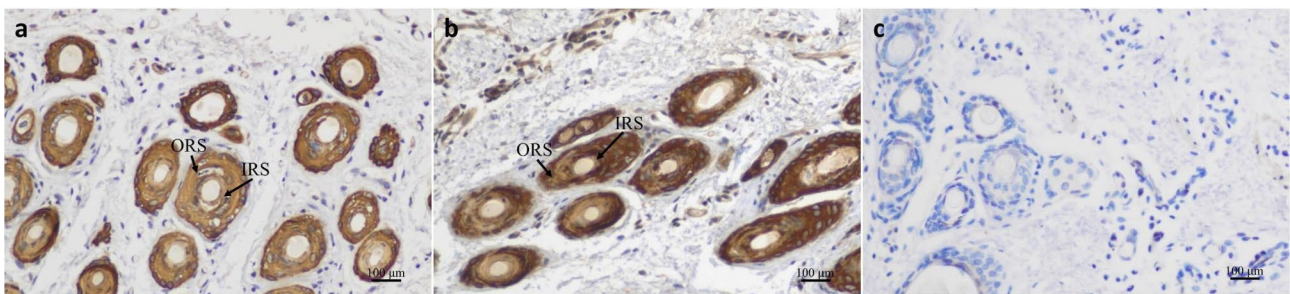


**Fig. 6** Localization of KRT71 in the skin of Inner Mongolian cashmere goats by immunohistochemistry. Brown cells were considered positive. **(a)**: Staining of KRT71 during anagen. (200 x); **(b)**: Staining for KRT71 during telogen. (200 x); **(c)**: Negative control. (200 x). Note: IRS, inner root sheath; ORT, outer root sheath

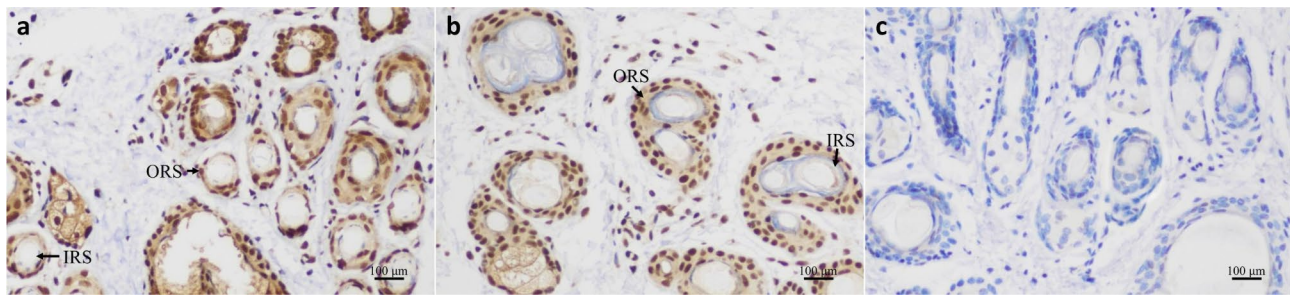


**Fig. 7** Localization of KRT82 in the skin of Inner Mongolian cashmere goats by immunohistochemistry. Brown cells were considered positive. (a): Staining of KRT82 during anagen. (200×); (b): Staining of KRT82 during telogen. (200×); (c): Negative control. (200 ×). Note: IRS, inner root sheath; ORT, outer root sheath

a transformation and forms an epithelial strand, which brings the dermal papilla close to the bulge [33]. In anagen, the regeneration of HFs is driven by stem cells in the bulge and coordinated by signal exchange from the dermal papilla niche [35, 36]. The signal between the bulge and dermal papilla is transported by extracellular exosomes in the skin [10, 15, 37]. In this study, the most enriched CC was extracellular exosomes, which is likely due to the reasons mentioned above. Extracellular exosomes have also been identified as a method of releasing cellular waste products [10]. Therefore, another reason for the greatest enrichment of CCs of extracellular exosomes might be that DRPs are involved mainly in BPs associated with metabolism. The importance of metabolism in the HF growth process was also confirmed through KEGG pathway analysis in this study. Metabolic regulation is a major driver of extracellular matrix production and degradation in fibroblasts [38]. In addition, adipocytes can drive HF growth by promoting the skin stem cell niche [39]. Fatty acids, which serve as important indicators of lipid breakdown, also have crucial functions in the development of HFs [40]. Furthermore, the DRPs identified in this study were enriched in fatty acid metabolism pathways, such as fatty acid degradation, fatty acid elongation, and unsaturated fatty acid biosynthesis. In the KEGG pathway analysis, the TCA cycle, oxidative phosphorylation, and PPAR signalling pathways were linked to fatty acid metabolism. The oxidation process of fatty acids is ultimately catabolized in the TCA cycle by oxidative phosphorylation in the mitochondria. Mitochondria were also enriched in the CC category according to the GO enrichment analysis. The PPAR signalling pathway participates in fatty acid oxidation and mitochondrial oxidative metabolism, and the four DRPs involved in the PPAR signalling pathway in our study were upregulated in anagen, which could promote the degradation of fatty acids and the TCA cycle [38]. These findings suggest that the abovementioned pathways are crucial for promoting the cyclic development of cashmere goat SHFs.

The majority of molecular processes take place within a cell in the presence of many proteins that are connected

by highly specific physical contacts. Hence, proteins rarely act alone. The interactions among these proteins can be called PPIs. MCODE analysis of the PPI prediction of our study revealed that the cluster with the highest score was mainly composed of r-proteins and EIFs. During cellular translation, r-proteins make up the subunits of the ribosome that work with rRNA [41], and EIFs also play an important role during this process; for example, the EIF3 family is critical in controlling translation initiation during the cell cycle, and the EIF4 family is related to protein synthesis [42, 43]. Therefore, our results indicated that DNA transcription and protein translation in the skin strongly increased during the HF growth period. The cluster with the second highest score was mainly composed of KRT family members, including KRT35, KRT73, KRT4, KRT82, KIF1, KRT71, KRT32, KRT85, KRT25, KRT39, KRT28, KRT74, and KRT27. KRTs are the main cytoskeletal proteins and not only play a role in support and mechanical resilience in the cell process but also play a very important role in the process of HF growth [44, 45]. The HF structure is composed of hair fibres, an IRS, an ORS, and a connective tissue sheath from the inside to the outside [4]. In human HFs, KRT25, KRT27, KRT28, KRT71, KRT73, and KRT74 are IRS proteins [46]. The immunohistochemical results of this study revealed that KRT25 was also expressed in the IRS of SHFs in the skin of Inner Mongolia cashmere goats. However, keratin 71 is expressed in both the IRS and ORS, which is different from its expression in single-coat mammals. For animals with single-coats, such as humans and mice, KRT71 is not only essential for the proper formation of the IRS but also indispensable for the correct moulding and growth of the hair shaft [47–49]. For the secondary hair follicles of Inner Mongolia cashmere goat skin, KRT71 may have more profound importance because of its wider expression, but its specific role still needs further research. In human HFs, KRT25, KRT27, KRT28, KRT32, KRT35, KRT82, and KRT85 are present in the hair-forming compartment, indicating that these keratins are involved in the synthesis and growth of human HFs [46]. Our results revealed that the main site of KRT82 expression is the

ORS of SHFs. The molecular mechanisms of SHF development in cashmere goat skin differ from those of single-coats animal HFs. However, the KRT family undoubtedly plays an irreplaceable and important role in the process of HF growth.

In addition to the protein cluster networks with high scores mentioned above, some proteins also needed special attention. For example, ANXA1, a calcium-dependent phospholipid binding protein, is upregulated during anagen. In the skin HFs of mice, ANXA1 participated in hair growth by influencing the proliferation of HF stem cells and the density of HFs. S100 family proteins must be mentioned. S100 proteins are a subgroup of Ca<sup>2+</sup>-binding proteins, some of which play an active role in the process of HF growth. For example, blockade of S100A3, an anagen-upregulated protein, can delay the entry of mouse HFs into the anagen period, reduce hair elongation, and decrease the number of subcutaneous HFs [50]. In our research, S100 protein family members could be seen among both anagen-upregulated and anagen-downregulated proteins, and studies on the transcriptome of cashmere goat skin SHFs revealed that although S100 gene family members participate in the growth process of SHFs, they have different biological functions from those of humans and mice [51, 52]. Our proteomic data also revealed that the S100 family plays an indispensable role in the periodic growth of cashmere goat skin SHFs.

## Conclusion

Cashmere, often known as soft gold, is produced in excess of 20,000 tons in China every year, and as a consequence, cashmere goats have become a major source of income for farmers and herders in northern China [53]. We compared the two periods of vigorous anagen and telogen variation in Inner Mongolia cashmere goat SHFs through the analytical method of proteomics. The proteins involved in the annual periodic growth of cashmere goat SHFs were revealed from the perspective of the proteome. Our immunohistochemistry data suggested that keratins have a relatively high cluster score, and the localization of KRT25, KRT71, and KRT82 revealed that these proteins were expressed in the SHFs of cashmere goat skin, although the specific expression sites were slightly different from those in humans and mice. The molecular mechanisms of SHF development in cashmere goat skin differ from those of single-coats animal HFs. Overall, these data provide new insight into the SHFs of cashmere goats; that is, the main SHF region and proteins involved in the initiation and continuation of SHF growth vary seasonally.

## Abbreviations

PHF	Primary hair follicle
SHF	Secondary hair follicle
HF	Hair follicle

FGF	Fibroblast growth factor
TGF- $\beta$	Transforming growth factor- $\beta$
BMP	Bone morphogenetic protein
TNF	Tumour necrosis factor
SWATH	Sequential windowed acquisition of all theoretical fragment ions
PCA	Principal component analysis
DRPs	Differentially regulated proteins
GO	Gene Ontology
BP	Biological process
MF	Molecular function
CC	Cellular component
PPI	Protein–protein interaction
WB	Western blotting
KRT	Keratin
EIF	Eukaryotic translation initiation factor
ORS	Outer root sheath
IRS	Inner root sheath

## Supplementary Information

The online version contains supplementary material available at <https://doi.org/10.1186/s12917-025-04608-z>.

Supplementary Material 1  
Supplementary Material 2  
Supplementary Material 3  
Supplementary Material 4

## Acknowledgements

We would like to thank the Aerbasi White Cashmere Goat Breeding Farm for providing samples to the authors. During the experiment, Jinquan Li provided the platform, whereas Zhihong Liu assisted with the design, conduct, analysis, evaluation, and interpretation of the data.

## Author contributions

RN and JL made substantial contributions to the conception and design of the experiments. Conceived and designed the experiments: ZL and JL. Performed the experiments: RN, CZ, MZ, YX, LM and LG. Analysed the data: RN, CZ, DM, LM, and YX. Wrote the paper: RN, YX, DM, QM, and LM. Critically revised the manuscript: HL and ZL. All the authors read and approved the final manuscript.

## Funding

This work was supported by the Northern Agriculture and Livestock Husbandry Technology Innovation Center (grant number BFGJ2022002), the National Key R&D Program of China (grant number 2021YFD1200901), the University Youth Science and Technology Talent Support Project of Inner Mongolia Autonomous Region (grant number NJYT23012), the Inner Mongolia Education Department Special Research Project For First Class Disciplines (grant number YLXKZX-NND-007), the Science and Technology Plan of Inner Mongolia Autonomous Region (grant number 2023KYPT0021) and the Doctoral Fund Project of Hulunbuir College (grant number 2020BS12).

## Data availability

The datasets are contained within the article and its accompanying files. The animal materials are available upon reasonable request from the respective author.

## Declarations

### Ethics approval and consent to participate

The experimental animals were privately owned by the Aerbasi White Cashmere Goat Breeding Farm, and our experiments were performed after informed consent was obtained from the farm. All the animal investigations followed the International Guiding Principles for Biomedical Research involving animals and were approved by the Special Committee on Scientific Research and Academic Ethics of Inner Mongolia Agricultural University, which is responsible for the approval of Biomedical Research Ethics of Inner

Mongolia Agricultural University (Approval No: (2020)056, project title: the International Guiding Principles for Biomedical Research involving animals, approval date: May 6th, 2020). The skin samples were taken aseptically using a biopsy punch under local anaesthetic to minimize pain and suffering to the animal.

#### Consent for publication

Not applicable.

#### Competing interests

The authors declare no competing interests.

Received: 21 October 2023 / Accepted: 19 February 2025

Published online: 27 February 2025

#### References

- Ansari-Renani, Reza H. Cashmere production, harvesting, marketing and processing by nomads of Iran - A review. *Pastoralism*. 2015;5(1):18.
- Scott W, Colin B. The Chinese cashmere industry: A global value chain analysis. *Dev Policy Rev*. 2014;32(5):589–610.
- Guangxian Z, Danju K, Sen M, Xingtao W, Ye G, Yuxin Y, Xiaolong W, Yulin C. Integrative analysis reveals ncRNA-mediated molecular regulatory network driving secondary hair follicle regression in cashmere goats. *BMC Genomics*. 2018;19(1):222.
- Jiang H. Hair follicle structure traits and developmental mechanisms of Chinese cashmere goat. *J Jilin Agric Univ*. 2012;34(05):473–82.
- Mingxing L, Xiang G, Li Y, Tian Y, Xiaohua L. Gsdma3 gene is needed for the induction of apoptosis-driven catagen during mouse hair follicle cycle. *Histochem Cell Biol*. 2011;136(3):335–43.
- Li Y, Fan W, Li C, Yin J, Zhang Y, Li J. Histomorphology research of the secondary follicle cycling of inner Mongolia cashmere goat. *Scientia Agricultura Sinica*. 2008;1(1):3920–6.
- Moore KA, Lemischka IR. Stem cells and their niches. *Science*. 2006;311(5769):1880–5.
- Millar SE. Molecular mechanisms regulating hair follicle development. *J Invest Dermatol*. 2002;118(2):216–25.
- Botchkarev VA, Kishimoto J. Molecular control of epithelial-mesenchymal interactions during hair follicle cycling. *J Invest Dermatol Symp Proc*. 2003;8(1):46–55.
- Carrasco E, Gonzalo S-H, Mittelbrunn M. The role of extracellular vesicles in cutaneous remodeling and hair follicle dynamics. *Int J Mol Encs*. 2019;20(11):2758.
- Schmidt-Ullrich R, Ralf P. Molecular principles of hair follicle induction and morphogenesis. *BioEssays*. 2027(3):247–61.
- Elaine F. Scratching the surface of skin development. *Nature*. 2007;445(7130):834.
- Mikkola ML. Genetic basis of skin appendage development. *Seminars Cell Dev Biol*. 2007;18(2):225–36.
- Huelsken J, Vogel R, Erdmann B, Cotsarelis G, Birchmeier W. Beta-Catenin controls hair follicle morphogenesis and stem cell differentiation in the skin. *Cell*. 2001;105(4):533–45.
- Lakshmi RR, Prakash G, Sun BS, Min OJ, Senthilkumar K, Won LH, Hwan BS, Liya Z, Kwan SY, Young JS, et al. Extracellular vesicles derived from MSCs activates dermal papilla cell in vitro and promotes hair follicle conversion from Telogen to anagen in mice. *Sci Rep*. 2017;7(1):15560.
- Zhihong L, Feng Y, Meng Z, Lina M, Haijun L, Yuchun X, Rile N, Tianyu C, Rui S, Yanjun Z. The intragenic mRNA-microRNA regulatory network during telogen-anagen hair follicle transition in the cashmere goat. *Sci Rep*. 2018;8(1):14227.
- Yu Tao YT, Li Geng LG, Liu Peng LP, Dong ShuTing DS, Zhang JiWang ZJ, Zhao Bin ZB. Proteomic analysis of maize reveals expression characteristics of Stress-Related proteins during grain development. *Sci Agric Sinica*. 2017;50(11):2114–28.
- Yansheng L, Ruth H, Silvia S, Jeppe JGLC, Roland M, Pedro B, Ruedi N. Quantitative measurements of N-linked glycoproteins in human plasma by SWATH-MS. *Proteomics*. 2013;13(8):1247–56.
- Gillet LC, Navarro P, Tate S, Röst H, Selevsek N, Reiter L, Bonner R, Aebersold R. Targeted data extraction of the MS/MS spectra generated by data-independent acquisition: a new concept for consistent and accurate proteome analysis. *Mol Cell Proteom*. 2012;11(6):O111.016717.
- Samuel P, Thomas EJ, C YE. Shotgun collision-induced dissociation of peptides using a time of flight mass analyzer. *Proteomics*. 2010;3(6):847–50.
- Venable JD, Dong MQ, Wohlschlegel J, Dillin A, Yates JR. Automated approach for quantitative analysis of complex peptide mixtures from tandem mass spectra. *Nat Methods*. 2004;1(1):39–45.
- Williams EG, Wu Y, Jha P, Dubuis S, Blattmann P, Argmann CA, Houten SM, Amariuta T, Wolski W, Zamboni N, Aebersold R, Auwerx J. Systems proteomics of liver mitochondria function. *Science*. 2016;352(6291):aad0189.
- Sun QL. RAPD analysis of nucleus DNA in different-area main cashmere breeds (groups) in China. Inner Mongolia Agricultural University; 2002.
- Yang F, Liu Z, Zhao M, Mu Q, Zhao Y. Skin transcriptome reveals the periodic changes in genes underlying cashmere (ground hair) follicle transition in cashmere goats. *BMC Genomics*. 2020;21(1):392.
- Zacchi LF, Schulz BL. SWATH-MS glycoproteomics reveals consequences of defects in the glycosylation machinery. *Mol Cell Proteom*. 2016;15(7):2435–47.
- Xiaolan Z, Qi B, Congjun J, Chen L, Yongfang C, Xiaoyun W, Chunnian L, Pengjia B, Ping Y. Genome-wide detection and sequence conservation analysis of long non-coding RNA during hair follicle cycle of Yak. *BMC Genomics*. 2020;21(1):681.
- Zhihao W, Li P, Huiying Z, Lei S, Yuehui W, Qi S, Chunjie G, Bin W, Xiujiao Q, Aiqun P. miR-128 regulates differentiation of hair follicle mesenchymal stem cells into smooth muscle cells by targeting SMAD2. *Acta Histochem*. 2016;118(4):393–400.
- Baptista TAM, Valerie H. Epithelial stem cells in adult skin. *Curr Top Dev Biol*. 2014;107:109–31.
- Higgins CA, Chen JC, Cerise JE, Jahoda CA, Christiano AM. Microenvironmental reprogramming by three-dimensional culture enables dermal papilla cells to induce de Novo human hair-follicle growth. *Proc Natl Acad Sci U S A*. 2013;110(49):19679–88.
- Eun LS, Aiko S, Meng Z, Yang JMD, Tudorita LSJKK. High Runx1 levels promote a reversible, more-differentiated cell state in hair-follicle stem cells during quiescence. *Cell Rep*. 2014;6(3):499–513.
- Lee J, Böske R, Tang PC, Hartman BH, Heller S, Koehler KR. Hair follicle development in mouse pluripotent stem Cell-Derived skin organoids. *Cell Rep*. 2020;22(1):242–54.
- Parodi C, Hardman JA, Allavena G, Marotta R, Catelani T, Bertolini M, Paus R, Grimaldi B. Autophagy is essential for maintaining the growth of a human (mini-)organ: evidence from scalp hair follicle organ culture. *PLoS Biol*. 2018;16(3):e2002864.
- Schneider MR, Schmidt-Ullrich R, Paus R. The hair follicle as a dynamic miniorgan. *Curr Biol*. 2009;19(3):R132–42.
- Bingbo S, Qiang D, Xiaolin H, Haijing Z, Yulin C. Tβ4-overexpression based on the piggybac transposon system in cashmere goats alters hair fiber characteristics. *Transgenic Res*. 2016;26(1):1–9.
- Greco V, Chen T, Rendl M, Schober M, Pasolli HA, Stokes N, et al. A two-step mechanism for stem cell activation during hair regeneration. *Cell Stem Cell*. 2009;4(2):155–69.
- Rezza A, Sennett R, Rendl M. Adult stem cell niches: cellular and molecular components. *Curr Top Dev Biol*. 2014;107:333–72.
- Ogawa M, Udono M, Teruya K, Uehara N, Katakura Y. Exosomes derived from Fisetin-Treated keratinocytes mediate hair growth promotion. *Nutrients*. 2021;13(6):2087.
- Xiao Z, Pamela P, Soltan GL, Kenneth Y, David G, Ralph G, Ian W, Hilary P, Ali H, Hee LJ, et al. Metabolic regulation of dermal fibroblasts contributes to skin extracellular matrix homeostasis and fibrosis. *Nat Metabolism*. 2019;1(1):147–57.
- Festa E, Fretz J, Berry R, Schmidt B, Rodeheffer M, Horowitz M, Horsley V. Adipocyte lineage cells contribute to the skin stem cell niche to drive hair cycling. *Cell*. 2011;146(5):761–71.
- Bejaoui M, Taarji N, Saito M, Nakajima M, Isoda H. Argan (*Argania Spinosa*) press cake extract enhances cell proliferation and prevents oxidative stress and inflammation of human dermal papilla cells. *J Dermatol Sci*. 2021;103(1):33–40.
- de la Cruz J, Karbstein K, Woolford JL Jr. Functions of ribosomal proteins in assembly of eukaryotic ribosomes in vivo. *Annu Rev Biochem*. 2015;84:93–129.
- Hori T, Kondo T, Tabuchi Y, Takasaki I, Zhao QL, Kanamori M, Yasuda T, Kimura T. Molecular mechanism of apoptosis and gene expressions in human lymphoma U937 cells treated with anisomycin. *Chemico-Biol Interact*. 2008;172(2):125–40.

43. Song S, Liu J, Zhang M, Gao X, Sun W, Liu P, Wang Y, Li J. Eukaryotic translation initiation factor 3 subunit B could serve as a potential prognostic predictor for breast cancer. *Bioengineered*. 2022;13(2):2762–76.
44. Ramms L, Fabris G, Windoffer R, Schwarz N, Springer R, Zhou C, Lazar J, Stiefel S, Hersch N, Schnakenberg U, Magin TM, Leube RE, Merkel R, Hoffmann B. Keratins as the main component for the mechanical integrity of keratinocytes. *Proc Natl Acad Sci U S A*. 2013;110(46):18513–8.
45. Guo T, Han J, Yuan C, Liu J, Niu C, Lu Z, Yue Y, Yang B. Comparative proteomics reveals genetic mechanisms underlying secondary hair follicle development in fine wool sheep during the fetal stage. *J Proteom*. 2020;223:103827.
46. Langbein L, Rogers MA, Praetzel-Wunder S, Helmke B, Schirmacher P. K25 (K25irs1), K26 (K25irs2), K27 (K25irs3), and K28 (K25irs4) represent the type I inner root sheath keratins of the human hair follicle. *J Invest Dermatol*. 2006;126(11):2377–86.
47. Aoki N, Sawada S, Rogers MA, Schweizer J, Shimomura Y, Tsujimoto T, Ito K, Ito M. A novel type II cytokeratin, mK6irs, is expressed in the Huxley and Henle layers of the mouse inner root sheath. *J Invest Dermatol*. 2001;116(3):359–65.
48. Kikkawa Y, Oyama A, Ishii R, Miura I, Amano T, Ishii Y, Yoshikawa Y, Masuya H, Wakana S, Shiroishi T, Taya C, Yonekawa H. A small deletion hotspot in the type II keratin gene mK6irs1/Krt2-6 g on mouse chromosome 15, a candidate for causing the wavy hair of the Caracul (Ca) mutation. *Genetics*. 2003;165(2):721–33.
49. Peters T, Sedlmeier R, Büssow H, Runkel F, Lüers GH, Korthaus D, Fuchs H, Angelis MHD, Stumm G, Russ AP, et al. Alopecia in a novel mouse model RCO3 is caused by mK6irs1 deficiency. *J Invest Dermatol*. 2003;121(4):674–80.
50. Guan W, Deng Q, Yu XL, Yuan YS, Gao J, Li JJ, Zhou L, Xia P, Han GY, Han W, Yu Y. Blockade of S100A3 activity inhibits murine hair growth. *Genet Mol Res*. 2015;14(4):13532–44.
51. Wu J, Li Y, Gong H, Wu D, Liu B. Molecular Basis of Maintaining Circannual rhythm in the skin gene expression of cashmere goat. *bioRxiv*. 2020;23–44.
52. Nocelli C, Cappelli K, Capomaccio S, Pasucci L, Mercati F, Pazzaglia I, et al. Shedding light on cashmere goat hair follicle biology: from morphology analyses to transcriptomic landscape. *BMC Genomics*. 2020;21(1):458.
53. Ge W, Zhang W, Zhang Y, Li F, Wang S, Liu J, Tan S, et al. A single-cell transcriptome atlas of cashmere goat hair follicle morphogenesis. *Genomics, Proteomics Bioinf*. 2021;19(3):437–51.

### Publisher's note

Springer Nature remains neutral with regard to jurisdictional claims in published maps and institutional affiliations.